CHEMISTRY
A EUROPEAN JOURNAL

DOI: 10.1002/chem.200600395

Unexpected Reaction of the Unsaturated Cluster Host and Catalyst $[Pd_3(\mu^3\text{-}CO)(dppm)_3]^{2+}$ with the Hydroxide Ion: Spectroscopic and Kinetic Evidence of an Inner-Sphere Mechanism**

Cyril Cugnet,[a] Dominique Lucas,*[a] Frédéric Lemaître,[a, b] Edmond Collange,[a] Armand Soldera,[b] Yves Mugnier,[a] and Pierre D. Harvey*[b]

Abstract: The title cluster, $[Pd_3(\mu^3\text{-}CO)(dppm)_3]^{2+}$ (dppm = bis(diphenylphosphino)methane), reacts with one equivalent of hydroxide anions (OH^-), from tetrabutylammonium hydroxide (Bu_4NOH), to give the paramagnetic $[Pd_3(\mu^3\text{-}CO)(dppm)_3]^{+}$ species. Reaction with another equivalent of OH^- leads to the zero-valent compound $[Pd_3(\mu^3\text{-}CO)(dppm)_3]^{0}$. From electron paramagnetic resonance analysis of the reaction medium using the spin-trap agent 5,5-dimethyl-1-pyrroline-*N*-oxide (DMPO), the 2-tetrahydrofuryl or methyl radicals, deriving from the tetrahydrofuran (THF) or dimethyl sulfoxide (DMSO) solvent, respectively, were detected. For both $[Pd_3(\mu^3\text{-}CO)(dppm)_3]^{2+}$ and $[Pd_3(\mu^3\text{-}CO)(dppm)_3]^{+}$, the mechanism involves, in a first equilibrated step, the formation of a hydroxide adduct, $[Pd_3(\mu^3\text{-}CO)(dppm)_3(OH)]^{(n-1)+}$ ($n = 1, 2$), which reacts irreversibly with the solvent. The kinetics were resolved by means of stopped-flow experiments and are consistent with the proposed mechanism. In the presence of an excess of Bu_4NOH, an electrocatalytic process was observed with modest turnover numbers (7–8). The hydroxide adducts $[Pd_3(\mu^3\text{-}CO)(dppm)_3(OH)]^{(n-1)+}$ ($n = 1, 2$), which bear important similarities to the well-known corresponding halide adducts $[Pd_3(\mu^3\text{-}CO)(dppm)_3(\mu^3\text{-}X)]^{n}$ (X = Cl, Br, I), have been studied by using density functional theory (DFT). Although the optimised geometry for the cluster in its +2 and 0 oxidation states (i.e., cation and anion clusters, respectively) is the anticipated μ^3-OH form, the paramagnetic species, $[Pd_3(\mu^3\text{-}CO)(dppm)_3(OH)]^{0}$, shows a μ^2-OH form; this suggests an important difference in electronic structure between these three species.

Keywords: cluster compounds · density functional calculations · hydroxide anions · palladium · solvent effects

[a] C. Cugnet, Dr. D. Lucas, Dr. F. Lemaître, Dr. E. Collange, Prof. Y. Mugnier
Université de Bourgogne, Laboratoire de Synthèse et Electrosynthèse Organométalliques
CNRS UMR 5188, Faculté des Sciences Mirande
9 Avenue Alain Savary, 21000 Dijon (France)
Fax: (+33) 380-396-091
E-mail: dominique.lucas@u-bourgogne.fr

[b] Dr. F. Lemaître, Prof. A. Soldera, Prof. P. D. Harvey
Université de Sherbrooke
Département de Chimie
Sherbrooke, Québec J1K 2R1 (Canada)
Fax: (+819) 821-8017
E-mail: pharvey@usherbrooke.ca

[**] dppm = bis(diphenylphosphino)methane.

Supporting information for this article is available on the WWW under http://www.chemeurj.org/ or from the author. It contains graphs of k_{obsc} and k_{obsd} versus $[OH^-]$, a simulation of the UV-visible spectrum evolution of $[Pd_3]^{2+}$ as a function of time in the presence of OH^- ($R = 40$), an EPR spectrum of the product from the stoichiometric reaction between $[Pd_3]^{2+}$ and OH^- ions in the presence of DMSO and DMPO, and representations for the HOMO and LUMO for $[Pd_3Br]^{+}$.

Introduction

Since the first report on the synthesis and characterisation of the $[Pd_3(\mu^3\text{-}CO)(dppm)_3]^{2+}$ cluster (notated $[Pd_3]^{n+}$ throughout this manuscript in which $n = 0, 1, 2$; dppm = bis-(diphenylphosphino)methane) in the 1980s, by Puddephatt et al.,[1–3] and its Pt analogue,[4] numerous and exhaustive studies on its reactivity and properties have appeared in the literature.[5–10] This cluster exhibits a triangular Pd_3 (M_3) centre with three dppm-supported M–M single bonds. Although a CO group caps one M_3 face, the other face is unsaturated, giving rise to rich coordination chemistry. The dppm phenyl groups form a cavity above this M_3 plane, limiting access to small substrates only.[11] Of particular interest in our current work is the binding of halide ions onto this $[Pd_3]^{2+}$ species leading to very stable architectures.[12] Related to this high affinity for halides, the cluster is also reactive towards the carbon–halogen bond, which led to important new catalytic processes in organic electrosynthesis.[13–15]

Because the OH^- anion is isolobal to halide anions,[16] the interactions between this anion and the title cluster should be similar, hence providing the corresponding OH^- species, which should exhibit analogous features as those for the halide adducts.[3,10]

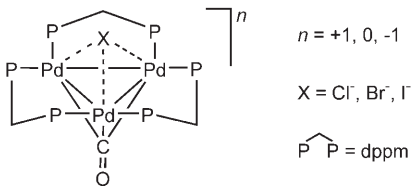

We report the reactivity of the OH^- ion with the $[Pd_3]^{2+}$ cluster under stoichiometric and electrocatalytic conditions, where, in an unexpected fashion, the cluster promotes the oxidation of the hydroxide ion in a solvent-dependent radical process. Supported by electron paramagnetic resonance (EPR) analysis and stopped-flow experiments, the mechanism implies the formation of $[Pd_3(OH)]^{(n-1)+}$ ($n=1$, 2) hydroxide adduct intermediates. The structures of these intermediates have been studied by using density functional theory (DFT). Although the monocationic species exhibits a μ^3-OH bridge, the $[Pd_3(OH)]^0$ species presents a μ^2-OH form.

Results and Discussion

Stoichiometric reactions with the title cluster: The rotating disk electrode (RDE) voltammogram of $[Pd_3]^{2+}$ in the absence and in the presence of varying amounts of OH^- ions is presented in Figure 1. In the absence of OH^- ions (Figure 1, line a), the voltammogram is characterised by two reduction waves of equal height, A_1 ($E_{1/2}=-0.29$ V vs. SCE) and A_2 ($E_{1/2}=-0.55$ V vs. SCE), corresponding to the two monoelectronic processes $[Pd_3]^{2+}+1e^-\rightarrow[Pd_3]^+$ and $[Pd_3]^+ +1e^-\rightarrow[Pd_3]^0$, respectively.[17] In the presence of one equivalent of OH^- ions (Figure 1, line b), the reduction wave A_1 disappears and the oxidation wave A'_1 appears, meaning that only the $[Pd_3]^+$ cluster species exists in solution. From the diffusion current measured on the plateau of wave A'_1, the reaction appears to be nearly quantitative. The presence of the +1 paramagnetic cluster was confirmed by using EPR spectroscopy (isotropic; septet relative intensity = 1:6:15:20:15:6:1; $g=2.065$, $a^{31P}=81.06$ G, $a^{105Pd}=8.13$ G).[9] On addition of another equivalent of OH^- ions (Figure 1, line c), the reduction wave A_2 disappears and the oxidation wave A'_2 appears, meaning that the $[Pd_3]^0$ cluster species was formed, also in a quantitative way. Its presence was confirmed by means of ^{31}P NMR spectroscopy ($\delta=14$ ppm).[17]

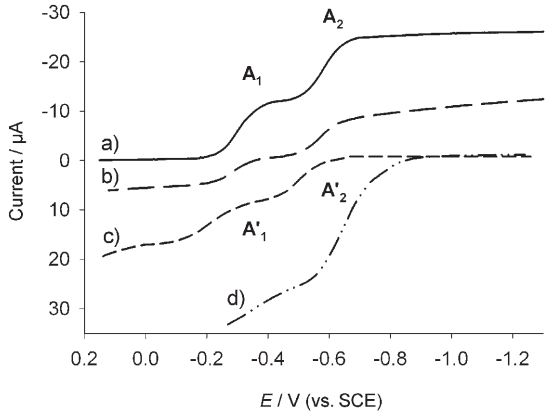

Figure 1. RDE voltammogram of $[Pd_3]^{2+}$ in THF/0.2 M Bu_4NPF_6 using a glassy carbon electrode: a) in the absence of OH^- ions; b) with 1 equiv of Bu_4NOH; c) with 2 equiv of Bu_4NOH; d) with 4 equiv of Bu_4NOH.

EPR investigation of the reaction intermediates: To detect the short-lived radical intermediates, the reactions were carried out after incorporation in the reaction medium of the spin-trap agent 5,5-dimethyl-1-pyrroline-*N*-oxide (DMPO). The addition of one equivalent of OH^- to a solution of $[Pd_3]^{2+}$ in THF led to the EPR recording depicted in Figure 2 (top). The seven-line spectrum of the EPR-active $[Pd_3]^+$ is observed together with a more narrow six-line signal attributed to a paramagnetic DMPO adduct. Addition of a second equivalent of OH^- led to the disappearance of the $[Pd_3]^+$ EPR signal, while the resonance of the DMPO adduct remained (Figure 2, bottom). In an independent experiment, OH^- was added to the electrochemically made $[Pd_3]^+$ in the presence of DMPO, and the same narrow EPR signal was produced.

Our experimental coupling constants ($a_\beta^H=19.1$ G, $a^N=13.93$ G) are clearly different from those expected for a DMPO–OH adduct (in toluene: $a_\beta^H=13.75$ G, $a^N=12.10$ G),[18] but are very close to those reported for a DMPO–alkyl adduct.[19]

Similar experiments were carried out in DMSO instead of THF. In this solvent, at each OH^- addition step, the methyl radical $CH_3^\bullet$ was demonstrated to be formed, unequivocally identified by EPR evidence of the DMPO–CH_3 adduct[20,21] (see the Supporting Information; Figure S1).

It is well known from literature findings that DMSO captures hydroxyl radicals as shown in Equation (1), which forms $CH_3^\bullet$ that can go on to react with DMPO [Eq. (2)]:

(1)

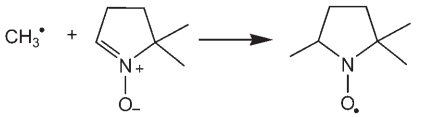

(2)

Similarly, $OH^\bullet$ may be able to react with THF, leading to the 2-tetrahydrofuranyl radical by H-atom abstraction at the α position according to Equation (3). The same reaction has

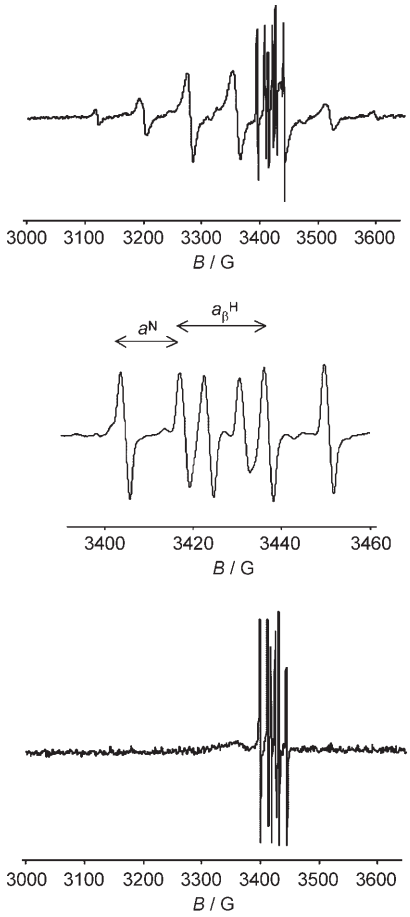

Figure 2. EPR spectra (isotropic) of the products from the stoichiometric reactions between $[Pd_3]^{2+}$ and 1 equiv of OH^- (top; the septet is due to the presence of $[Pd_3]^+$), and between $[Pd_3]^{2+}$ and 2 equiv of OH^- (bottom). Inset: enlargement of the signal associated with the DMPO adduct.

been reported to be achieved by the *tert*-butyloxyl radical *t*BuO$^\bullet$.[22]

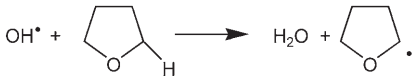

(3)

Consequently, in the trapping experiment, the observed radical does correspond to the DMPO–THF adduct [Eq. (4)]. Indeed our experimental values agree quite well with those in the literature (in benzene: $a_\beta^H = 17.92$ G, $a^N = 14.12$ G).[19]

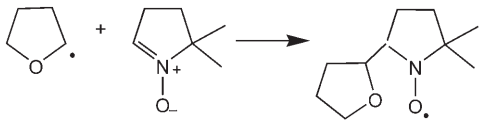

(4)

After the first attempt, these results led us to believe that the hydroxyl radical was the species responsible for the radical solvent fragmentation. To test this, OH$^\bullet$ was generated by ultraviolet photolysis of hydrogen peroxide[23] in THF or DMSO also containing DMPO, and in fact, the same spectra as above were obtained.

Mechanistic aspects: Directly inspired by its behaviour towards halides, we propose that in a first, equilibrated step, the hydroxide anion must be added to the cluster, in the +2 or +1 state, to form an intermediate adduct, as shown in Equation (5):

$$[Pd_3]^{n+} + OH^- \rightleftharpoons [Pd_3(OH)]^{(n-1)+} \quad n = 1, 2 \tag{5}$$

The proposal is consistent with the high affinity of $[Pd_3]^{2+}$ and $[Pd_3]^+$ clusters for small anions, particularly for halides, for which the electronic shell is the same as that for OH^-. There are just a few examples of low-valent Pd–hydroxy complexes with respect to Pd^{II} species. These examples include the d^9–d^9 binuclear species $[Pd_2(\mu\text{-}CH_2CHCHCH_2)(\mu\text{-}OH)(PPh_3)_2]PF_6$[24] and $[Pd_2(dppm)_2(OH)_2]$.[25] The OH^- binding constant is expected to be larger for $[Pd_3]^{2+}$ than for $[Pd_3]^+$, as deduced from the analogy with halide behaviour.[8] Accordingly, $[Pd_3]^{2+}$ reacts significantly faster with OH^- than $[Pd_3]^+$, as the latter does not give any reaction before the former is fully exhausted.

Another possibility lies in the nucleophilic addition of OH^- to the coordinated CO. Indeed, the reaction between hydroxide ions and transition-metal carbonyls has been known for some time[26] and usually affords a hydroxycarbonyl intermediate that evolves into a metal hydride species and carbon dioxide as shown in Equation (6):

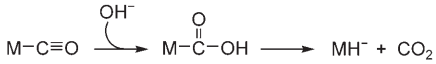

(6)

This reaction also applies to the triangular cluster series $[M_3(CO)_{12}]$ (M = Fe, Ru or Os).[27] However, in our case, such a process concurrent to [Eq. (5)] can be ruled out as the identity of the products ($[Pd_3]^+$ or $[Pd_3]^0$ depending on whether 1 or 2 equiv of OH^- are added on $[Pd_3]^{2+}$) demonstrates that the carbonyl ligand remains totally unchanged: as evidence, the attack of OH^- takes place exclusively at the more electrophilic cationic trimetallic centre.

As soon as the reaction in Equation (5) is accepted as the first step, to explain the observed reactivity, the host–guest assemblies $[Pd_3(OH)]^{(n-1)+}$ ($n = 1, 2$), unlike the very stable halide adducts, must undergo a subsequent reaction. In order to solve this point, the first question was, is the free hydroxyl radical OH$^\bullet$ truly formed through this reaction? Because the EPR results showed evidence that radicals deriving from the solvent (THF or DMSO) can also be obtained independently by direct reaction of OH$^\bullet$ with the solvent (see above), its formation can reasonably be postulat-

ed. In this way, the second step would simply consist of the OH$^{\bullet}$ dissociation from the hydroxide adducts [Eq. (7)], followed by the solvent attack [Eqs. (1) and (3)].

$$[Pd_3(OH)]^{(n-1)+} \rightarrow [Pd_3]^{(n-1)+} + OH^{\bullet} \quad n = 1, 2 \tag{7}$$

However, basic thermodynamic calculations demonstrate that Equation (7) is too uphill in energy to exist separately. Indeed, by summing Equations (5) and (7), one obtains the following electron-transfer reaction [Eq. (8)]:

$$[Pd_3]^{n+} + OH^- \rightarrow [Pd_3]^{(n-1)+} + OH^{\bullet} \quad n = 1, 2 \tag{8}$$

The standing free-energy change (ΔG_8° (kJmol^{-1}), in which the subscript refers to the equation number) is expressed as a function of the standard redox potentials $E^{\circ}([Pd_3]^{n+}/[Pd_3]^{(n-1)+})$ and $E^{\circ}(OH^{\bullet}/OH^-)$:

$$\Delta G_8^{\circ} = F\Delta E^{\circ}$$
$$\Delta G_8^{\circ} = 96.5\ [E^{\circ}(OH^{\bullet}/OH^-) - E^{\circ}([Pd_3]^{n+}/[Pd_3]^{(n-1)+})]$$

$E^{\circ}([Pd_3]^{n+}/[Pd_3]^{(n-1)+})$ are simply identified from the half-wave potentials[28–30] $E_{1/2}(A_1)$ (−0.29 V versus SCE) and $E_{1/2}(A_2)$ (−0.55 V versus SCE).

$E^{\circ}(OH^{\bullet}/OH^-)$ is more difficult to evaluate with certainty, but the half-wave potential measured from the voltammogram of a solution of free OH$^-$ on glassy carbon, $E_{1/2}$ = 0.48 V versus SCE, gives a rough estimate of this standard potential. Glassy carbon is an electrode material that does not interact with the electrogenerated OH$^{\bullet}$ radicals and so is appropriate for this determination.[31] In acetonitrile (also an aprotic solvent in which the hydroxide ion is poorly solvated), the same procedure leads to $E_{1/2}$ = 0.68 V versus SCE. Overall, ΔG_8° ($n=2$) ≈ 74 kJ mol^{-1} and ΔG_8° ($n=1$) ≈ 99 kJ mol^{-1}.

As stated above, Equation (5) should be energetically favoured ($\Delta G_5^{\circ} < 0$), which means that ΔG_7° will be even more positive than ΔG_8° ($\Delta G_8^{\circ} = \Delta G_5^{\circ} + \Delta G_7^{\circ}$). Because, for an elementary reaction, the driving force (ΔG°) sets a minimum activation energy ($E_a^{\neq}$), clearly, the reaction in Equation (7) is unlikely, both thermodynamically and kinetically.

If the intermediate formation of OH$^{\bullet}$ is ruled out, what can be the alternative pathway? Three species were identified to be involved in the formation of the final reaction products: the cluster, the hydroxide anion and the solvent. As $[Pd_3(OH)]^{(n-1)+}$ ($n=1, 2$) was demonstrated to be unable to dissociate by itself, at this stage, we tentatively propose that the solvent comes into play. So, the second step will be reformulated as shown in Equations (9) and (10) for reaction in THF or DMSO, respectively.

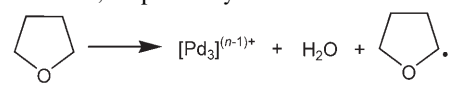

(9)

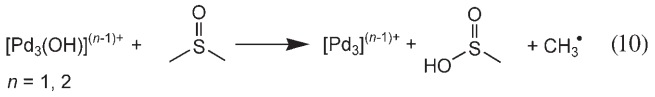

(10)

By simply considering the bond that is broken (C–H in THF; S–C in DMSO) and the one that is formed (O–H in THF; S–O in DMSO), the integration of the solvent undoubtedly provides a significantly less positive free-energy change,[32] and supposedly, a lower activation barrier. The reaction probably arises through the initial formation, of an activated complex between the hydroxide adduct and the solvent S {$[Pd_3(OH)]^{(n-1)+}$—S}, from which the bond reorganisation would operate, although no information is provided on the details of the process.

The oxidation of OH$^-$ by transition-metal complexes is not unprecedented, but the mechanism is markedly different from ours.[33,34] The closest reaction to ours is achieved by neutral tris(dithiolene) complexes of molybdenum(VI) or tungsten(VI) [Eq. (11)].

$$[ML_3] + OH^- \rightarrow [ML_3]^- + {}^1/_2H_2O_2 \quad L = \text{dithiolene ligand} \tag{11}$$

This reaction produces, in addition to the anionic reduced complex, hydrogen peroxide, which was not detected in our case. But, analogously to our mechanism, the first step consists of reversible binding of the hydroxide ion to the metallic centre; this leads to a species formulated as $[ML_3(OH)]^-$.

Stopped-flow experiments: Stopped-flow experiments were carried out to get supplemental evidence of the proposed mechanism. In Figure 3 (top, with $R=40$ as an example; R = [OH$^-$]/[cluster]), several zones of evolution are depicted. First, at $t=0$ (no OH$^-$ added) the initial cluster exhibits its characteristic $\lambda=495$ nm band. For $t=1$ ms, a rapid spectroscopic change was observed and the $\lambda=495$ nm band vanished, indicating a rapid reactivity with OH$^-$ ions. An intermediate band is apparent at $\lambda=460$ nm for $R<10$, but appears as a shoulder for larger R values (Figure 3, bottom). Still for $R=40$, between $1<t<100$ ms, a rapid spectral evolution was noted and the shoulder of variable intensity was still present in the $\lambda=450$–500 nm range. For $t>100$ ms, the spectral evolution is much slower and weak spectra variations are noted.

The first step of the $[Pd_3]^{2+}$/OH$^-$ reaction is the host–guest reaction as indicated in Equation (5) and Scheme 1a. We define k_a and k_{-a} [Eq. (12)] as the equilibrium rate constants for this process, with

$$K_a = \frac{k_a}{k_{-a}} = \frac{[[Pd_3(OH)]^+]}{[[Pd_3]^{2+}][OH^-]} \tag{12}$$

This hypothesis is consistent with the presence of an isosbestic point around $\lambda=440$ nm (Figure 3, bottom) for spectra recorded at $t=1$ ms for various R values. The crossing point at $\lambda=360$ nm is not an isosbestic point like that we observe

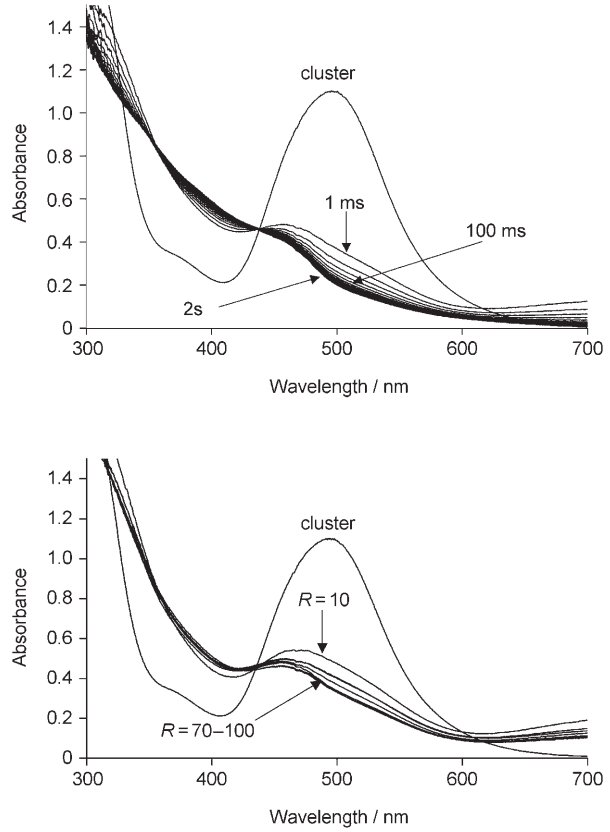

Figure 3. UV-visible study of the interaction between $[Pd_3(\mu\text{-CO})(dppm)_3]^{2+}$ and OH^- in THF. Top: representative spectra of the time evolution in an $R=40$ experiment. Bottom: initial spectrum (1 ms) from $R=10$ to $R=100$ experiments.

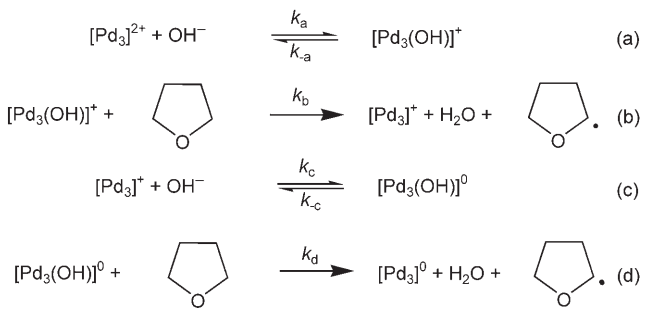

Scheme 1. Sequence of reactions of the palladium complexes with OH^- anions in THF.

in the spectra simulation (Figure S2; Supporting Information). The rate of this reaction is too fast to be measured with stopped-flow experiments and we could not determine the observed rate constant ($k_{obsa}=k_a[OH^-]+k_{-a}$).

The apparent equilibrium constant, K_{obsa}, for a constant $[OH^-]$ is defined as shown in Equation (13) in which D is the absorbance:

$$K_{obsa}=K_a[OH^-]=\frac{[[Pd_3(OH)]^+]}{[[Pd_3]^{2+}]}=\frac{(D_{[Pd_3]^{2+}}-D_{eq})}{(D_{eq}-D_{[Pd_3(OH)]^+})} \qquad (13)$$

D_{eq} corresponds to the first spectrum recorded at 1 ms, $D_{[Pd_3]^{2+}}$ is the absorbance in the initial cluster spectrum ($t=0$) and $D_{[Pd_3(OH)]^+}$ is the equilibrium spectrum obtained at saturation. It is assumed that saturation is reached at $R=100$. The equilibrium spectrum is then recalculated by using Equation (14):

$$D_{eq}=\frac{D_{[Pd_3]^{2+}}+K_{obsa}D_{[Pd_3(OH)]^+}}{1+K_{obsa}} \qquad (14)$$

in which K_{obsa} is reintroduced as an approximated value, and D_{eq} is then subtracted from the experimental value. By minimising the added squares of this difference for various $[OH^-]$ as a function of K_{obsa} (Excel Solver), one obtains the optimum value of K_{obsa}. Figure 4 (top) shows the linear dependence of K_{obsa} on $[OH^-]$, the slope of which gives $K_a=1051\pm45$. Interestingly, this value agrees quite well with that measured for the association of Cl^- with $[Pd_3]^{2+}$ ($K\approx2000$).[35]

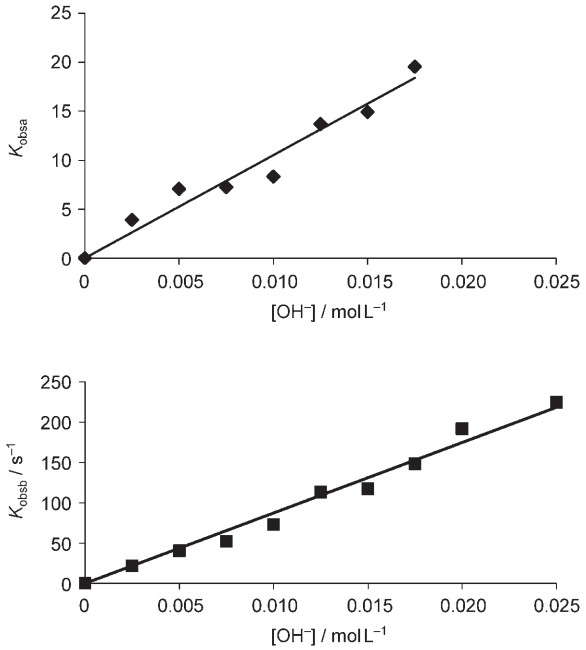

Figure 4. Equilibrium and rate constants for the evolution of $[Pd_3(\mu\text{-CO})(dppm)_3]^{2+}$. Top: apparent equilibrium constant for the initial reaction. Bottom: pseudo-first-order rate constant for the second step of the reaction.

The rest of the analysis was based on Scheme 1, with all reactions being pseudo first order and where $k_{obsb}\gg k_{obsc}\gg k_{obsd}$. Host–guest reactions are defined by K_a and K_c.

Because k_a and k_{-a} are large, the reaction in Scheme 1a has always reached equilibrium when the subsequent reaction takes place (Scheme 1b). As $[[Pd_3(OH)]^+]=K_a[[Pd_3]^{2+}][OH^-]$, the rate for this second reaction, v, is expressed by $v=k_b[[Pd_3(OH)]^+]=k_bK_a[[Pd_3]^{2+}][OH^-]$. So, equation b is always $[OH^-]$ dependent, behaving linearly such that $k_{obsb}=k_bK_a[OH^-]$, as observed in Figure 4 (bottom). From this plot, one extracts $K_ak_b=8690\pm236\ s^{-1}$ and $k_b=8.3\pm0.6\ s^{-1}$.

For the reactions in Scheme 1c and d, the same treatment is applied because the mechanism is identical to that in reactions a and b (addition of a hydroxide ion followed by an irreversible reaction of the resulting adduct with the solvent).

For the host–guest reaction between $[Pd_3]^+$ and OH^- (Scheme 1c), K_c is defined as shown in Equation (15):

$$K_c = \frac{[[Pd_3(OH)]]}{[[Pd_3]^+][OH^-]} = \frac{k_c}{k_{-c}} \quad (15)$$

If $k_{obsc} > k_{obsd}$, the analysis can be performed by assuming that reaction c is independent. If so, $k_{obsc} \approx k_c[[Pd_3]^+][OH^-] + k_{-c}$. In fact, the graph of k_{obsc} versus $[OH^-]$ is linear (see Figure S3; Supporting Information) and provides the following data: $k_c = 367 \pm 26\ mol^{-1}\ L\ s^{-1}$, $k_{-c} = 4.3 \pm 0.2\ s^{-1}$ and $K_c = k_c/k_{-c} = 85 \pm 10$.

As expected, K_c is significantly lower than K_a; as the complex charge is reduced by one unity, the trimetallic centre becomes less electrophilic.

For reaction d, using a similar treatment as that used for $k_{b,}$ we obtain $k_{obsd} = k_d K_c[OH^-]$. The graph of k_{obsd} versus $[OH^-]$ is also linear (Figure S3; Supporting Information), and one extracts $k_d = 0.5 \pm 0.1\ s^{-1}$.

The spectra of all the species involved in Scheme 1 have been extrapolated with Specfit[36] (see Figure S4; Supporting Information) and we observe that the spectra of $[Pd_3]^+$, $[Pd_3(OH)]^0$ and $[Pd_3]^0$ are not very different from each other, which explains the low accuracy of the rate constant values for reactions c and d.

Additionally, to support these assignments, $[Pd_3]^+$ and $[Pd_3]^0$ were also prepared from the reductive electrolysis of $[Pd_3]^{2+}$ stopped at a transfer of one and two faradays per mole of cluster, respectively. Their UV-visible spectra (recorded in situ by means of an immersion probe) were found to be identical to those calculated. By using the calculated spectra and the equilibrium rate constants obtained for these experiments, the evolution of the UV-visible spectra as a function of time was calculated for $R = 40$ (Figure S2; Supporting Information). The simulation agrees well with the experimental results of Figure 3 (top).

Electrochemical catalysis: Because the $[Pd_3]^0$ cluster can be electrochemically oxidised back to $[Pd_3]^{2+}$ either from $[Pd_3]^+$ or $[Pd_3]^0$,[17] it offered us the opportunity to study the catalysed oxidation of OH^-.

In the presence of an excess of OH^- ions, the $[Pd_3]^{2+}$ species becomes $[Pd_3]^0$, as previously stated, but the RDE voltammogram exhibits a fusion of the reduction waves A'_1 and A'_2, as well as a shift towards more negative potentials accompanied with an increase in current (Figure 1, line d). This result indicates the presence of a catalytic process occurring on the electrochemical timescale. Despite the fact that the stoichiometric reaction (a) is faster than reaction (b), both the one- and two-electron processes (Scheme 2a and b) should be considered.

Using a carbon-mesh working anode electrode with an applied potential of −0.1 V versus SCE, the oxidation of the

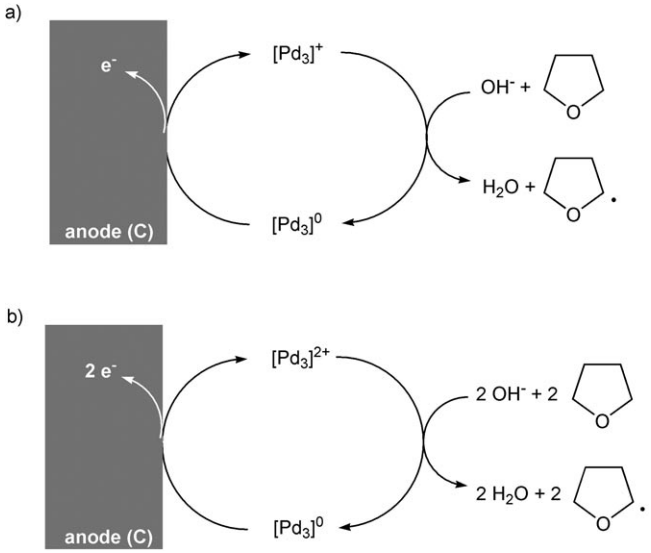

Scheme 2. a) One- and b) two-electron processes for the catalysed oxidation of OH^- anions in THF.

$[Pd_3]^0$ and $[Pd_3]^+$ species into the $[Pd_3]^{2+}$ cluster in the presence of 20 equiv of OH^- ions, was performed by monitoring the charge (Q) and by using Equation (16):

$$\text{Turnover number} = Q_{exptl}/Q_{cluster} \quad (16)$$

in which $Q_{cluster}$ is the required electric charge necessary to oxidise $[Pd_3]^+$ into $[Pd_3]^{2+}$ or $[Pd_3]^0$ into $[Pd_3]^{2+}$, and Q_{exptl} is the measured electric charge. The turnover numbers are 14–16 and 7–8 for mechanism (a) or (b) in Scheme 2, respectively; these values are very low and witness the occurrence of competitive processes leading to the deactivation of the cluster catalyst.

Computations: The key intermediates in Equations (5) and (9), $[Pd_3(OH)]^n$ ($n = +1, 0, -1$), were studied by means of DFT, particularly with respect to structures and bonding as the OH^- fragment is capable of acting as a two-, four- or six-electron donor with Pd centres.[25,37,38] To test the methodology, geometry optimisations were performed on a parent compound, $[Pd_3Br]^+$, for which the X-ray structure is known from this laboratory.[39] The data are presented in Table 1, and are compared with the computed three possible oxidation states of the cluster. Four functionals under the generalised gradient-corrected approximation, GGA, were tested: PW91, BP, BLYP, PBE. Results using the Perdew–Wang[40] functional best mimicked the experimental data with a reliability factor of 2.3%. It should be pointed out that BP exhibits a reliability factor of 2.4%. Accordingly, the PW91 functional was used in the study of $[Pd_3(\mu_3\text{-}Br)(\mu_3\text{-}CO)]$ because only comparisons with experimental data were envisioned; whereas the two functionals PW91 and BP were selected for the study of $[Pd_3(CO)(OH)]$, unless stated otherwise. Nevertheless, differences among the internal pa-

Table 1. Comparison of selected X-ray and DFT average distances (d in Å) for the $[Pd_3(\mu^3\text{-Br})(\mu^3\text{-CO})(dppm)_3]^{n+}$ clusters ($n=+1, 0, -1$).

			PW91	
	X-ray ($n=+1$)	DFT ($n=+1$)	DFT ($n=0$)	DFT ($n=-1$)
d(Pd–Pd)	2.592(10)	2.635	2.744	2.970
d(Pd–P)	2.311(6)	2.316	2.300	2.302
d(Pd–C)	2.142(3)	2.202	2.164	2.174
d(Pd···Br)	2.940	2.867	2.902	2.975
d(C=O)	1.104(10)	1.176	1.175	1.194
			BP	
	X-ray ($n=+1$)	DFT ($n=+1$)	DFT ($n=0$)	DFT ($n=-1$)
d(Pd–Pd)	2.592(10)	2.649	2.770	2.978
d(Pd–P)	2.311(6)	2.325	2.305	2.310
d(Pd–C)	2.142(3)	2.203	2.170	2.179
d(Pd···Br)	2.940	2.879	2.910	2.9995
d(C=O)	1.104(10)	1.177	1.176	1.195
			BLYP	
	X-ray ($n=+1$)	DFT ($n=+1$)	DFT ($n=0$)	DFT ($n=-1$)
d(Pd–Pd)	2.592(10)	2.692	2.820	3.061
d(Pd–P)	2.311(6)	2.375	2.365	2.352
d(Pd–C)	2.142(3)	2.241	2.208	2.211
d(Pd···Br)	2.940	2.968	3.007	3.122
d(C=O)	1.104(10)	1.176	1.184	1.195
			PBE	
	X-ray ($n=+1$)	DFT ($n=+1$)	DFT ($n=0$)	DFT ($n=-1$)
d(Pd–Pd)	2.592(10)	2.647	2.770	2.970
d(Pd–P)	2.311(6)	2.320	2.298	2.307
d(Pd–C)	2.142(3)	2.202	2.163	2.173
d(Pd···Br)	2.940	2.873	2.900	2.967
d(C=O)	1.104(10)	1.177	1.175	1.195

rameters between the different functionals are small (< 0.06 Å).

The optimised geometry exhibits the anticipated μ^3-Br form of the $[Pd_3(\mu^3\text{-Br})]$ skeleton, and the comparison of the X-ray data with the calculated bond lengths of the $[Pd_3Br]^+$ species exhibit good agreements. The calculated Pd–P bond length is essentially identical to the average experimental value taking into account the uncertainties, and the other computed Pd atom distances were calculated to be located between 0.06 and 0.07 Å away from the X-ray results.

Representations of the highest occupied molecular orbital (HOMO) and lowest unoccupied molecular orbital (LUMO) for $[Pd_3Br]^+$ to be used as a comparison with the $[Pd_3(OH)]^+$ cluster are provided in the Supporting Information. The HOMO is composed of a Br^- p atomic orbital (lone pair) along with Pd d and O p (π) atomic orbitals. This orbital exhibits important $Br^-\cdots Pd$ antibonding interactions. The LUMO is composed of Pd d and P p (lone pairs) atomic orbitals, and an O p contribution. Almost no contribution from the Br^- ion was found. The LUMO is characterised by antibonding Pd–Pd and Pd–P interactions and bears an important resemblance to its homologue reported for the unsaturated $[Pd_3]^{2+}$ cluster,[7,11] indicating that the presence of Br^- does not affect these frontier MOs.

Upon addition of one and two electrons to the $[Pd_3Br]^+$ clusters, two distances, Pd–Br and Pd–Pd, experience an important change, while the others are little affected. The Pd–Pd bond length increases with the sequential one-electron reductions, going from 2.635 to 2.970 Å, which is consistent with the Pd–Pd antibonding nature of the LUMO.[7,11] The distance 2.970 Å is very similar to that reported for the d^{10}–d^{10} $[Pd_2(dppm)_3]$ binuclear complex, in which no Pd–Pd bond exists (Pd···Pd = 2.956(1) Å, X-ray data).[41] The Pd···Br interactions are primarily due to ionic bonding. As the charge on the $[Pd_3]^n$ centre decreases (n: $+2\rightarrow+1\rightarrow0$), the Pd···Br separation increases. This result is consistent with the decrease in the binding constant between halides and $[Pd_3]^n$ ($n=0$–2).[8,15] These effects are also anticipated for the OH adduct.

The optimised geometries (PW91) for the $[Pd_3(OH)]^n$ species ($n=+1$, 0, -1) exhibit the μ^3-OH bridge for the diamagnetic cases ($n=+1$ and -1), and the μ^2-OH one for the neutral cluster (Scheme 3). The reason for this selectivity is unknown, but fluxionality of the OH^- ligand around the $[Pd_3]^+$ frame is still possible.

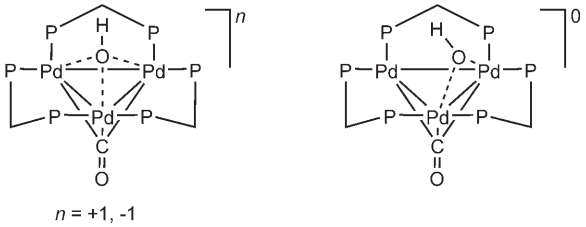

Scheme 3. The optimised geometries for the $[Pd_3(OH)]^n$ species showing the μ^3-OH bridge for the diamagnetic cases (left), and the μ^2-OH bridge for the neutral cluster (right).

The calculated bond lengths for the $[Pd_3(CO)(OH)]$ skeleton are presented in Table 2 (PW91 and BP). The first important feature is the covalent nature of the Pd–O bond in the $[Pd_3(OH)]^+$ cluster, as the computed distance is 2.364 Å, which is close to the range of distances that is normally encountered for Pd^{II}– and Pd^{I}–OH bonds (2.05–2.25 Å, Cambridge Structural Database). This property eases the electron transfer in an inner-sphere process. The second important feature is that reduction of the cluster leads to the same anticipated effect discussed above for the Pd–Pd and Pd–X bonds (here X = OH).

Representations of the HOMO and LUMO for $[Pd_3(OH)]^+$ are provided in Figure 5. The HOMO bears important similarities to that of $[Pd_3Br]^+$ discussed above. The LUMO is almost identical to that for $[Pd_3Br]^+$ (and $[Pd_3]^{2+}$). The main conclusion is that OH^- binds the $[Pd_3]^{2+}$ centre in the same way as Br^- (or any halogen anion).

The surprise comes from the paramagnetic neutral cluster $[Pd_3(OH)]^0$ for which the OH^- ligand acts as a μ^2-bridge as stated (C_s symmetry). The singly occupied molecular orbital (SOMO) is represented in Figure 6. The very small atomic contribution of OH^- indicates that the electronic density is primarily located on the $[Pd_3]^+$ frame. This observation was corroborated by spin density calculations. The delocalisation appears to be the reason for the greater stability of this

Table 2. Comparison of selected DFT average distances (d in Å) for the $[Pd_3(\mu_3\text{-}CO)(dppm)_3(\mu\text{-}OH)]^{n+}$ clusters ($n=+1, 0, -1$).

		PW91	
	$n=+1$	$n=0$	$n=-1$
d(Pd–Pd)	2.666	2.756 (μ-OH)	3.077
		2.777	
d(Pd–P)	2.310	2.335/2.269/2.303	2.293
d(Pd–C)	2.202	2.149–2.170	2.193
d(Pd–O)	2.364	2.328 (μ-OH)	2.412
		3.534	
d(C=O)	1.179	1.177	1.195
		BP	
	$n=+1$	$n=0$	$n=-1$
d(Pd–Pd)	2.685	2.755 (μ-OH)	3.090
		2.781	
d(Pd–P)	2.325	2.340/2.269/2.307	2.294
d(Pd–C)	2.217	2.154–2.175	2.206
d(Pd–O)	2.372	2.336 (μ-OH)	2.417
		3.520	
d(C=O)	1.180	1.179	1.195

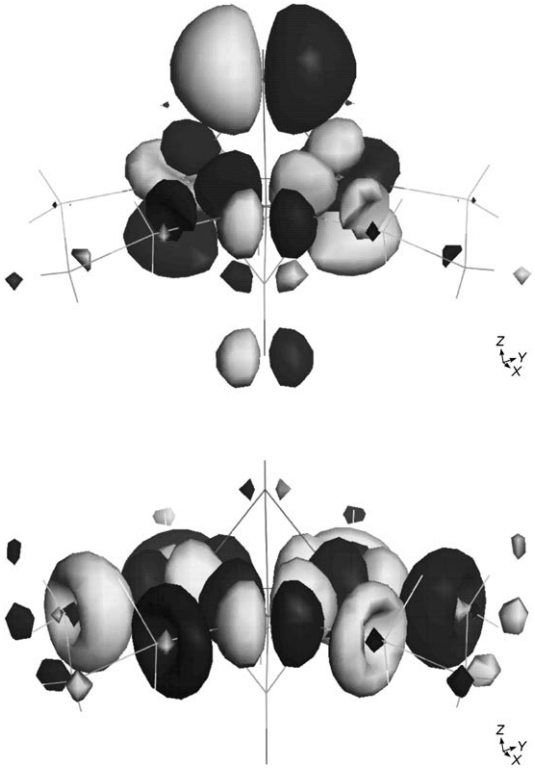

Figure 5. Representations of the HOMO (top) and LUMO (bottom) for $[Pd_3(OH)]^+$ (PW91).

form of spin distribution. The computed Pd–O bond lengths did not vary very much on going from $[Pd_3(OH)]^+$ to the neutral cluster (2.364 to 2.328 Å for PW91; 2.372 to 2.336 Å for BP), and are consistent with the very little atomic contribution of the OH^- ligand to the frontier MOs. The calculated Pd–P distances undergo lengthening and shortening for the bonds placed perpendicular and parallel to the Pd–μ-OH–Pd fragment, respectively, indicating that the covalent nature of the Pd–O bond influences the back bonding of the

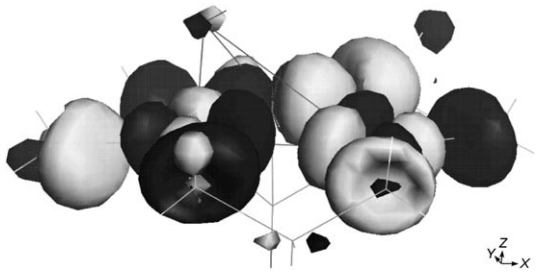

Figure 6. Representation of the SOMO for $[Pd_3(OH)]^0$ (PW91).

Pd–P frames. The Pd–P bonds for the unsaturated Pd metal exhibit a distance (2.303 Å for PW91; 2.307 Å for BP) that is intermediate to the four others.

Upon addition of an extra electron, the optimised geometry for the neutral $[Pd_3(OH)]^0$ cluster exhibits the C_{3v} local symmetry geometry (Figure 7). The computed nonbonding

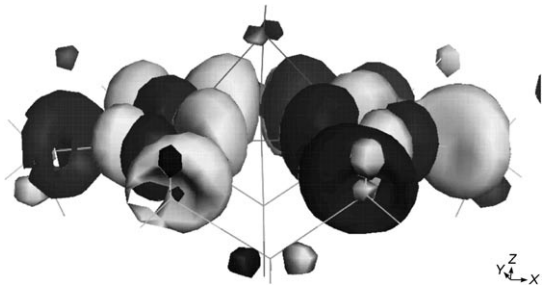

Figure 7. Representation of the HOMO for $[Pd_3(OH)]^-$ (PW91).

Pd···Pd separation (3 Å) as well as the bonding Pd–P, Pd–C and C=O distances compare favourably to that for the corresponding $[Pd_3Br]^-$ cluster (Table 1), indicating the minimal effect that the OH^- and Br^- ligands have on the Pd_3 frame. Again, the LUMO, SOMO and HOMO for $[Pd_3(OH)]^n$ ($n=+1, 0, -1$, respectively), originate from the same interactions, with little or no interaction from the substrate.

These species, $[Pd_3(OH)]^n$ ($n=+1, 0, -1$), are very unstable, as demonstrated by the stopped-flow experiments, but calculations suggest that they exhibit an optimised geometry (i.e., a geometry of minimum energy). This observation is consistent with the stopped-flow experiments in which different absorption spectra were time resolved.

Experimental Section

Materials: The $[Pd_3(CO)(dppm)_3][PF_6]_2$ complex was prepared according to literature procedures.[1,5,12] THF was distilled under Ar over Na–benzophenone (Aldrich), DMSO was distilled under Ar over CaH_2 and Bu_4NOH and DMPO were purchased from Aldrich and used as received.

Apparatus: NMR spectra were measured on a Bruker WM 300 spectrometer (^{31}P NMR: 121.497 MHz). The reference was the residual non-deuterated solvent. The chemical shifts are reported with respect to

H_3PO_4 (^{31}P NMR). EPR measurements were carried out on a Bruker ESP 300 spectrometer; field calibration was made with diphenyl picryl hydrazyl (DPPH; $g = 2.0037$). The UV-visible spectra were carried out on a Cary 50 (Varian) spectrophotometer with a fibre-optic probe directly immersed in the reaction medium.

Electrochemical experiments: All manipulations were performed by using Schlenk techniques in an atmosphere of dry, oxygen-free argon gas at room temperature. The supporting electrolyte was degassed under vacuum before use and then solubilised at a concentration of 0.2 mol L^{-1}. For cyclic voltammetry experiments, the concentration of the analyte was nearly 10^{-3} mol L^{-1}. Voltammetric analyses were carried out in a standard three-electrode cell with a Tacussel PJT24-1 potentiostat connected to a waveform generator (Tacussel GSTP4). The reference electrode was a saturated calomel electrode (SCE) separated from the solution by a sintered glass disk. The auxiliary electrode was a platinum wire. For all voltammetric measurements, the working electrode was a vitreous carbon electrode ($\varphi = 3$ mm). In these conditions, when operating in THF, the formal potential for the ferrocene$^{+/-}$ couple was found to be $+0.56$ V versus SCE. The controlled potential electrolysis was performed with an Amel 552 potentiostat coupled with an Amel 721 electronic integrator. High-scale electrolyses were performed in a cell with three compartments separated by fritted glasses of medium porosity. A carbon gauze was used as the working electrode, a platinum plate as the counter electrode and a saturated calomel electrode as the reference electrode.

Stopped-flow experiments: The stopped-flow kinetic runs were carried out, at 15 °C, with a Hitech SF-61-DX2 apparatus coupled with a Hitech diode-array UV-visible spectrophotometer. To minimise oxidation reactions in the stopped-flow apparatus, relatively concentrated cluster solutions ($2 \times 2.5 \times 10^{-4}$ mol L^{-1}, $\approx$maximum solubility) were used. Under these conditions, the cell was kept small at 1.5 mm. The dead time was $\approx$1 ms. Kinetic runs were analysed by using Specfit,[36] while the fitting of the observed first-order rate and equilibrium constants was carried out with Excel Solver. The standard deviation of the determined parameters was obtained by using the Solver Aide macro.[42] The cluster solution (5×10^{-4} mol L^{-1}) was mixed with a Bu_4NOH-containing solution in a way that the concentration ratio $R = [Bu_4NOH]/[cluster] = 1, 5, 10, 20, \ldots 80, 100$. The data analysis was performed by assuming a pseudo-first-order reaction ($R \geq 10$).

Computations: All calculations were performed by using DFT, implemented in the DMol3 program of Accelrys Inc. in the Material Studio environment, on dual AMD Athlon processors. The density functional semicore pseudopotential (DSPP)[43] was used to model Pd: core-electrons effects (those within the 4f orbital) were replaced by a simple potential corrected by some degree of relativistic effects. Under the generalised gradient-corrected approximation (GGA), four functionals were tested: PW 91,[40] BP,[40,44] BLYP,[44,45] and PBE.[46] A Fermi smearing of 0.002 hartrees and a real-space cutoff of 4 Å were also chosen. The selected numerical basis set DNP is equivalent in size and quality to the 6-31G** basis set. The precision was set as follows: a SCF tolerance of 10^{-6} hartrees; a geometry optimisation accuracy of 10^{-3} Å for the displacement, 10^{-3} hartrees $Å^{-1}$ for the gradient and 10^{-6} hartrees for the energy. The computations were performed using $PH_2CH_2PH_2$ due to the great demand in CPU (Central Process Units) time with dppm. No symmetry restrictions were imposed in any calculations.

Conclusion

An astonishing reaction of the palladium cluster with the hydroxide ion has been evidenced. The mechanism involves the formation of a hydroxide adduct in a preliminary step. This intermediate is highly reactive and undergoes a further reaction with the solvent in a way that has no precedent in the literature. This fact may suggest that some literature reports deserve to be revisited to address the possibility of solvent involvement. Attempts to make these processes catalytic by taking advantage of the electrochemical reversibility of the one- and two-electron $[Pd_3]^n$ redox processes provided only modest results under the experimental conditions investigated. The DFT calculations predict a clear resemblance in electronic and atomic structure between the halide adducts ($[Pd_3X]^+$) and $[Pd_3(OH)]^+$. The similarity stops there as the latter cluster proves very unstable experimentally. In addition, the one- and two-electron reductions led to other unstable species for which one of them, $[Pd_3(OH)]^0$, exhibits a different geometry (μ^2- instead of μ^3-) according to DFT calculations.

Acknowledgements

P.D.H. thanks NSERC (Natural Sciences and Engineering Research Council of Canada) for funding. Y.M. is grateful to CNRS (Centre National de la Recherche Scientifique) for funding.

[1] L. Manojlovic-Muir, K. W. Muir, B. R. Lloyd, R. J. Puddephatt, *J. Chem. Soc. Chem. Commun.* **1983**, 1336–1337.
[2] B. R. Lloyd, R. J. Puddephatt, *Inorg. Chim. Acta* **1984**, *90*, L77–L78.
[3] R. J. Puddephatt, L. Manojlovic-Muir, K. W. Muir, *Polyhedron* **1990**, *9*, 2767–2802.
[4] G. Ferguson, B. R. Lloyd, R. J. Puddephatt, *Organometallics* **1986**, *5*, 344–348.
[5] L. Manojlovic-Muir, K. W. Muir, B. R. Lloyd, R. J. Puddephatt, *J. Chem. Soc. Chem. Commun.* **1985**, 536–537.
[6] R. Provencher, K. T. Aye, M. Drouin, J. Gagnon, N. Boudreault, P. D. Harvey, *Inorg. Chem.* **1994**, *33*, 3689–3699.
[7] P. D. Harvey, R. Provencher, *Inorg. Chem.* **1993**, *32*, 61–65.
[8] F. Lemaître, D. Lucas, D. Brevet, A. Vallat, P. D. Harvey, Y. Mugnier, *Inorg. Chem.* **2002**, *41*, 2368–2373.
[9] D. Brevet, D. Lucas, H. Cattey, F. Lemaître, Y. Mugnier, P. D. Harvey, *J. Am. Chem. Soc.* **2001**, *123*, 4340–4341.
[10] P. D. Harvey, Y. Mugnier, D. Lucas, D. Evrard, F. Lemaître, A. Vallat, *J. Cluster Sci.* **2004**, *15*, 63–90.
[11] P. D. Harvey, S. Hubig, T. Ziegler, *Inorg. Chem.* **1994**, *33*, 3700–3710.
[12] B. R. Lloyd, L. Manojlovic-Muir, K. W. Muir, R. J. Puddephatt, *Organometallics* **1993**, *12*, 1231–1237.
[13] F. Lemaître, D. Lucas, Y. Mugnier, P. D. Harvey, *J. Org. Chem.* **2002**, *67*, 7537–7540.
[14] F. Lemaître, D. Lucas, K. Groison, P. Richard, Y. Mugnier, P. D. Harvey, *J. Am. Chem. Soc.* **2003**, *125*, 5511–5512.
[15] D. Brevet, Y. Mugnier, F. Lemaître, D. Lucas, S. Samreth, P. D. Harvey, *Inorg. Chem.* **2003**, *42*, 4909–4917.
[16] T. A. Albright, J. K. Burdett, M. H. Whangbo, *Orbital Interactions in Chemistry*, Wiley, New York, **1984**.
[17] I. Gauthron, Y. Mugnier, K. Hierso, P. D. Harvey, *Can. J. Chem.* **1997**, *75*, 1182–1187.
[18] D. L. Haire, Y. Kotake, E. G. Janzen, *Can. J. Chem.* **1988**, *66*, 1901–1911.
[19] E. G. J. Janzen, J. I. P. Liu, *J. Magn. Reson.* **1973**, *9*, 510–512.
[20] S. Pou, C. L. Ramos, T. Gladwell, E. Renks, M. Centra, D. Young, M. S. Cohen, G. M. Rosen, *Anal. Biochem.* **1994**, *217*, 76–83.
[21] D. A. Stoyanovsky, Z. Melnikov, A. I. Cederbaum, *Anal. Chem.* **1999**, *71*, 715–721.
[22] A. J. Clark, S. Rooke, T. J. Sparey, P. C. Taylor, *Tetrahedron Lett.* **1996**, *37*, 909–912.
[23] M. G. Steiner, C. F. Babbs, *Arch. Biochem. Biophys.* **1990**, *278*, 478–481.
[24] M. Abdul Jalil, T. Nagai, T. Murahashi, H. Kurosawa, *Organometallics* **2002**, *21*, 3317–3322.

[25] M. L. Kullberg, F. R. Lemke, D. R. Powell, C. P. Kubiak, *Inorg. Chem.* **1985**, *24*, 3589–3593.
[26] F. Calderazzo in *Organic Synthesis via Metal Carbonyls* (Eds.: I. Wender, P. Pino), Interscience, New York, **1968**.
[27] D. J. Darensbourg, B. J. Baldwin, J. A. Froelich, *J. Am. Chem. Soc.* **1980**, *102*, 4688–4694.
[28] The standard potential is related to $E_{1/2}$ by the equation: $E^{\circ} = E_{1/2} - (RT/nF) \times \ln (D_R/D_O)^{1/2} (f_0/f_R)$ in which R is the gas constant, T is the temperature, n is the number of exchanged electrons, F is the Faraday constant, D_O and D_R are the diffusion coefficients for the oxidised and reduced forms, respectively, and f_O and f_R are the activity coefficients for the oxidised and reduced forms, respectively. The second term on the right side of the equation is small, especially in the case of a large-sized molecule like the cluster.
[29] P. Delahay, *New Instrumental Methods in Electrochemistry*, Interscience, New York, **1954**.
[30] D. E. Richardson, H. Taube, *Inorg. Chem.* **1981**, *20*, 1278–1285.
[31] D. T. Sawyer, P. Chooto, P. K. S. Tsang, *Langmuir* **1989**, *5*, 84–89.
[32] *Handbook of Chemistry and Physics*, **1983–1984**, p. F187–F190.
[33] A. Cervilla, F. Pérez-Plà, E. Llopis, M. Piles, *Dalton Trans.* **2004**, 1461–1465.
[34] P. K. Gosh, B. S. Brunschwing, M. Chou, M. Creutz, N. Sutin, *J. Am. Chem. Soc.* **1984**, *106*, 4772–4783.
[35] P. D. Harvey, K. Hierso, P. Braunstein, X. Morise, *Inorg. Chim. Acta* **1996**, *250*, 337–343.
[36] R. A. Binstead, B. Jung, A. D. Zuberbühler, Specfit/32, version 3.0, Spectrum Software Associates (Chapel Hill, NC), **2000**.
[37] O. Espinet, C. Hernandez, J. M. Martin-Alvarez, J. A. Miguel, *Inorg. Chem.* **2004**, *43*, 843–845.
[38] A. Klein, A. Dogan, M. Feth, H. Betagmolli, *Inorg. Chim. Acta* **2003**, *343*, 189–201.
[39] D. Lucas, F. Lemaître, B. Gallego-Gómez, C. Cugnet, P. Richard, Y. Mugnier, P. D. Harvey, *Eur. J. Inorg. Chem.* **2005**, 1011–1018.
[40] J. P. Perdew, Y. Wang, *Phys. Rev. B* **1992**, *45*, 13244–13249.
[41] R. V. Kirss, R. Eisenberg, *Inorg. Chem.* **1989**, *28*, 3372–3378.
[42] R. De Levie, *J. Chem. Educ.* **1999**, *76*, 1594–1598.
[43] B. Delley, *Phys. Rev. B* **2002**, *66*, 155125.
[44] A. D. Becke, *J. Chem. Phys.* **1988**, *88*, 2547–2553.
[45] C. Lee, W. Yang, R. G. Parr, *Phys. Rev. B* **1988**, *37*, 785–789.
[46] J. P. Perdew, K. Burke, M. Ernzerhof, *Phys. Rev. Lett.* **1996**, *77*, 3865–3868.

Received: March 21, 2006
Published online: August 9, 2006

